Korean J. Chem. Eng., 37(5), 898-904 (2020)
DOI: 10.1007/s11814-020-0506-5

pISSN: 0256-1115
eISSN: 1975-7220

Composite of nanocrystalline cellulose with tin dioxide as Lightweight Substrates for high-performance Lithium-ion battery

Quang Nhat Tran*, Il Tae Kim*, Jaehyun Hur*, Ji Hyeon Kim*, Hyung Wook Choi, and Sang Joon Park*,†**

*Department of Chemical and Biological Engineering, Gachon University, Seongnam, Gyeonggi-do 13120, Korea
**Department of Electrical Engineering, Gachon University, Seongnam, Gyeonggi-do 13120, Korea
(*Received 12 October 2019 • accepted 6 February 2020*)

Abstract−Nanocrystalline Cellulose (CNC) has smoother surfaces, better optical transparency and higher mechanical strength in comparison with various cellulose fibers. These properties combined with their low cost, light weight, and flexiblility indicate CNC's great potential as an attractive candidate for preparation of carbon materials, which can be promising electrode for Lithium-ion batteries. However, CNC cannot be directly used in battery fabrication because of its electrically non-conductive property. Wherefore, using pyrolysis to convert CNC into conductive materials is extensively investigated. In our study, high temperature range is used to convert nanocrystalline cellulose into highly conductive carbon material and used in Lithium-ion batteries. The nanocellulose powder after pyrolysis from 800 °C and 1,600 °C is used as active material in Lithium-ion battery electrodes, and the results obtained show a good electrochemical performance with stable cycling capacity. Following, the carbon network obtained through the pyrolysis (800 °C and 1,600 °C) of nanocrystalline cellulose incorporation with tin dioxide (SnO_2) was also used as electrode material in Lithium-ion batteries, resulting in stability, outstanding capacity and better performance in comparison with other carbon-based materials.

Keywords: Lithium-ion Batteries, Nanocrystalline Cellulose, Pyrolysis, Carbon Based Conductive Materials, Tin Dioxide

INTRODUCTION

The sustainable development and environmental friendliness in energy storage technology has been receiving more attention recently. Based on different kinds of energy storage technologies, electrochemical energy storage technology has been commonly used in various applications. Electrochemical energy storage devices can be divided into two groups, including battery and supercapactor based on its balance between energy and power density. Carbon is the commonest material used for electrodes in both commercial batteries and supercapacitors; moreover, carbon materials from renewable natural sources, feedstocks, green synthesis route and environmentally friendly components, such as wood, biomass can be available at low cost and be produced using simple pyrolysis and hydrothermal carbonization [1-4].

In this respect, nanocellulose with most common types cellulose nanocrystals (CNC) is one of the cheapest, most abundant, biodegradable, and sustainable nanomaterials that shows great potential as an attractive candidate for preparation of carbon materials. It can be a promising electrode for battery technology because of its excellent flexibility, large specific surface area, optical transparency, and outstanding mechanical strength for both films and aerogel forms. It also shows great potential when used as an additional substance to improve the formation of flexible electrode materials. In addition, using nanocellulose from renewable sources can decrease the total electrode cost and can be more competitive for electricity storage on a large scale. However, nanocellulose is an insulating material, which reduces the conductivity of the electrode and may lead to more challenges when applied for high power application. To strengthen the properties and conductivity of CNC, many approaches have been applied to convert nanocellulose to more conductive materials and used them in batteries [4-8]. Moreover, despite the abundance of sodium and calcium elements in the Earth's crust, lithium ion batteries commonly have higher efficiency than calcium ion batteries and store more power than sodium ion batteries [9-11].

First, we studied the behavior of using high temperatures ranging (800 °C-1,600 °C) to convert nanocellulose into highly conductive carbon materials and used them in Lithium-ion batteries. Following, the combination of nanocellulose powder after pyrolysis as active material with Super P, PVDF and N-methyl pyrolidone served as electrodes on Cu foils used in Lithium-ion batteries.

Tin dioxide (SnO_2) is popular among metal-oxide electrode materials with its outstanding electrochemical performance. Moreover, owing to its non-toxic property, low cost synthesis and high theoretical capacity make it more considered for use as electrode in Lithium-ion batteries [12-15]. Nano-size structure of SnO_2 is used to decrease the volume variation during charge and discharge process to improve the electrochemical performance of the electrode [16-18]. However, nanostructured SnO_2 is easy to agglomerate, which reduces the specific surface area of the active materials, leading to the decline of capacity and cell performance. To overcome this issue, a composite material of SnO_2 and pyrolyzed CNC has been created to utilize the area of electrode specific surface and combine the advantanges of both materials to enhance the electrical conductivity of the composite material [19-21].

In this work, we synthesized a composite material of pyrolyzed

†To whom correspondence should be addressed.
E-mail: psj@gachon.ac.kr

CNC and SnO_2 (CNC-SnO_2) to introduce pyrolyzed CNC as the supporting structure framework for the performance of SnO_2 and also as a conductive material. The composite materials (CNC-SnO_2) served as electrode materials in Lithium-ion batteries.

EXPERIMENT DETAILS

1. Pyrolysis of Nanocrystalline Cellulose

Nanocrystalline cellulose (CNC) suspension, received from SK innovation, was sonicated for 10 min, vacuum filtrated to obtain a CNC film. After freeze drying, the film was further heated to 800 °C (CNC-800) and 1,600 °C (CNC-1600) in nitrogen for 2 h (heating rate: 5 °C min^{-1}).

2. Synthesis of CNC-SnO_2 Material

50 mg pyrolyzed CNC film (CNC-800 & CNC-1600) was dispersed in 60 ml ethanol/water (2 : 4 v/v) and ultrasonicated for 2 hrs (100 W). 0.55 g CTAB and 2 ml HCl (37 wt%) were added and kept stirred for 30 min. 50 mg $SnCl_2 \cdot 2H_2O$ was added and keep stirred for 1 hr. Afterstirring for 1 hr the mix solution was transferred into 100 ml Teflon stainless autoclave and kept in an oven 24 hrs at 120 °C. The formed samples from autoclave after the reaction finished were centrifugated at 8,000 rpm with ethanol and DI water to remove impurities. Finally, the CNC-SnO_2 material (CNC 800-SnO_2 & CNC 1600-SnO_2) was dried at 60 °C overnight.

3. Materials Characterization

The crystal structure of CNC before and after the pyrolysis was carried out with Cu Kα monochromatic radiation using X-ray powder diffraction (XRD, RIGAKU/DMAX2200, Japan) of Smart Materials Research Center for IoT at Gachon University. A rate of 1.0° min^{-1} between 20-80° ranges was used to scan the 2θ Bragg angles. A Raman scattering measurement was carried out using a micro-Raman instrument (ANDOR Monora500i) equipped with a 533-nm He-Ne laser (12 mW), with an integration time of 5 s and one cycle of accumulation. The morphology of the as-obtained samples was characterized by scanning electron microscopy (SEM; Hitachi S-4700) and transmission electron microscopy (TEM; FEI, Tecnai, F30S-Twin).

4. Electrochemical Performance Measurement

An argon-fill glove box was emplyed to fabricate coin cells (CR2032) which were used to directly evaluate the electrochemical performance of the obtained materials. A slurry containing of 70 wt% obtained materials, 15 wt% PVDF, 15 wt% Super P and N-methy pyrrolidone was covered Cu foils for preparing the electrode to evaluate the cell electrochemical performance. The electrodes were dried at 60 °C in an oven for 3 h and following at 70 °C in vacuum oven overnight. The cells consisted of polyethylene membrane as the separator, lithium foil as the counter electrode and solution of 1 M $LiPF_6$ in ethylene carbonate/diethylene carbonate (1 : 1 in volume) as the electrolyte. The cell performance experiments were calculated by a battery cycler (WBCS3000, WonAtech) system and 100 mA g^{-1} at 0.01-2.0 V (vs. Li/Li^+) constant current density was applied.

RESULTS AND DISCUSSION

The nanocrystalline cellulose XRD profiles were obtained from

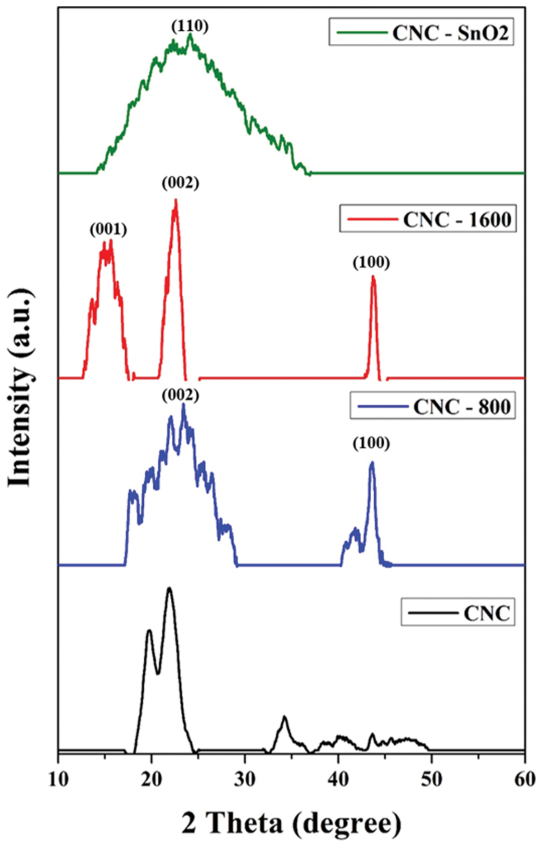

Fig. 1. XRD patterns of nanocrystalline cellulose (CNC), CNC pyrolyzed at 800 °C, CNC pyrolyzed 1,600 °C and CNC-SnO_2.

Fig. 1 with observered carbon residual peaks after pyrolysis at 800 °C and 1,600 °C. The XRD patters of CNC were identified as native cellulose and cellulose, and the characteristic profile well agreeed with ICSD data (PDF 03-0289 and 03-0228) for native cellulose and cellulose with observed peaks at 19.8°, 22.6°, 34°, 40.2° and 44°. The peak of characteristic sharpness indicates that CNC is highly crystal structure, in agreement with the report from SK innovation. The XRD profile from the pyrolysis of CNC has broad reflection peaks at 24° and 43°, which corresponded to the lattice planes of graphite (002) and (100), respectively; in agreement with previous reports [4,22]. From the last figure (CNC-SnO_2), the observed diffraction peak of CNC-SnO_2 is well consistent with the diffraction peaks of SnO_2 of ICSD data (PDF 21-1250), and value of the peak was obtained at 26° for the 2θ angle. Nevertheless, the observed peaks of CNC for the CNC-SnO_2 XRD patters were not clearly explained by the cover of SnO_2 on the surface of CNC film, which caused the disappearance of CNC peaks in CNC-SnO_2 XRD profile.

The surface appearance of CNC, CNC after pyrolysis and CNC combined with SnO_2 particles is shown in Fig. 2. Comapared with CNC (Fig. 2(a)), CNC-800 (Fig. 2(b)) shows uniform and higher porous surface. Moreover, the surface of CNC-1600 (Fig. 2(c)) shows heterogeneous surface with some holes. These important results lead to better performance in LIBs for CNC-800 when nanocellulose powder after pyrolysis is applied as electrode. Besides, Fig. 2(d) clearly shows that SnO_2 nanoparticles were deposited in CNC-SnO_2 composite without agglomeration to improve the electrochemical

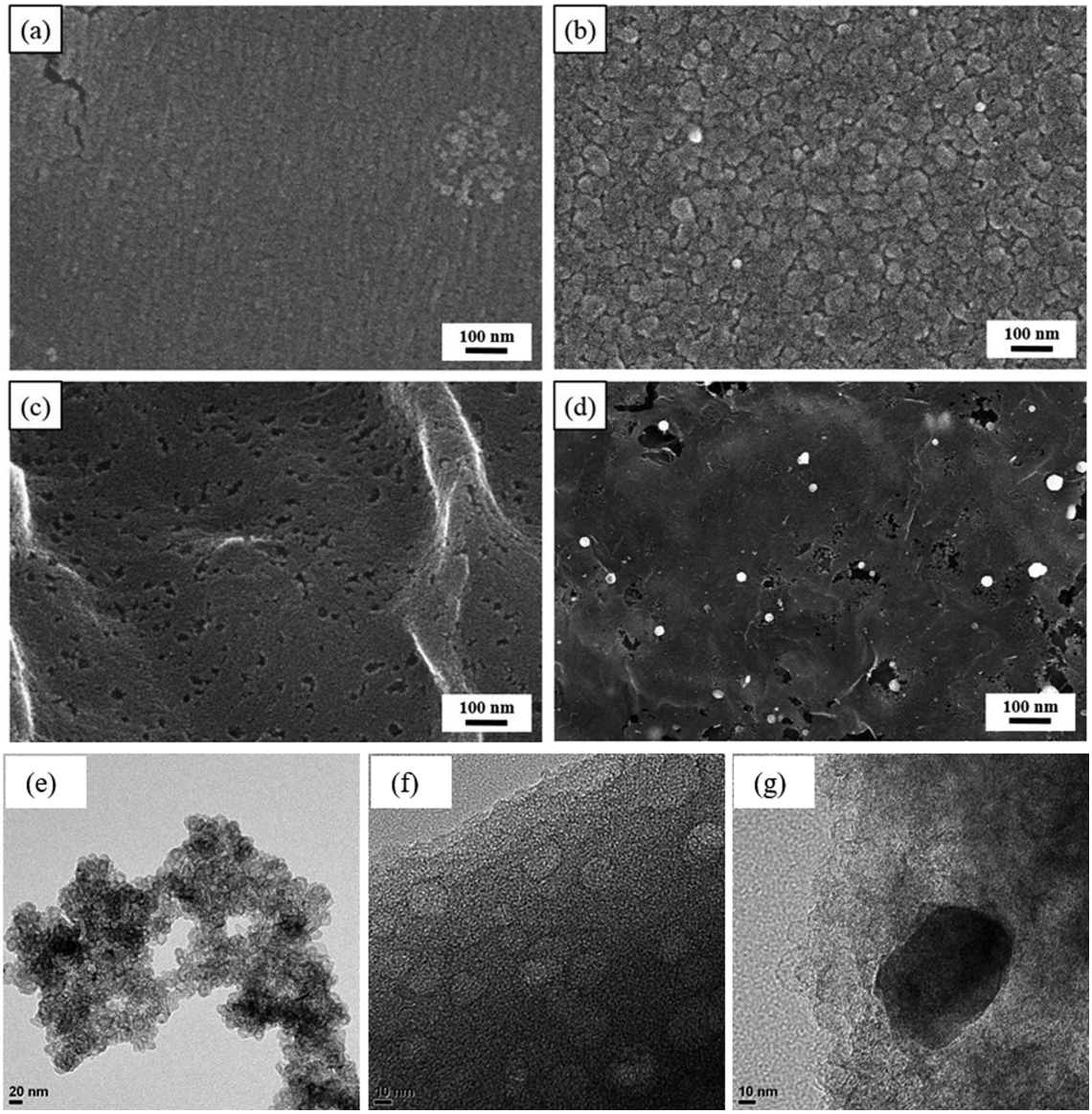

Fig. 2. SEM images of (a) nanocrystalline cellulose (CNC), (b) CNC pyrolyzed at 800 °C, (c) 1,600 °C, (d) CNC-SnO_2 and TEM images of (e) nanocrystalline cellulose (CNC), (f) CNC pyrolyzed at 800 °C, (g) 1,600 °C.

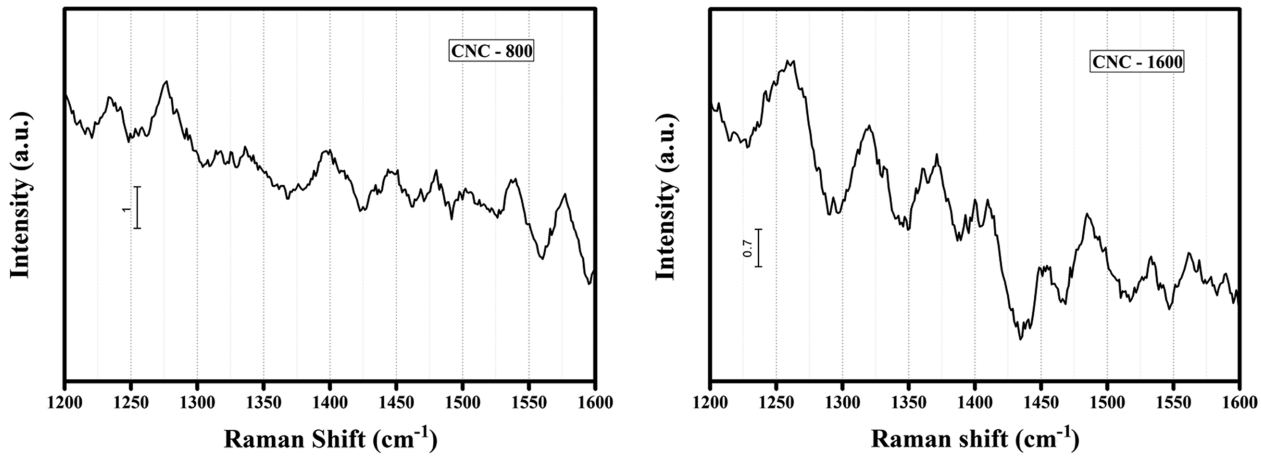

Fig. 3. Raman spectra of nanocrystalline cellulose pyrolyzed at 800 °C and 1,600 °C.

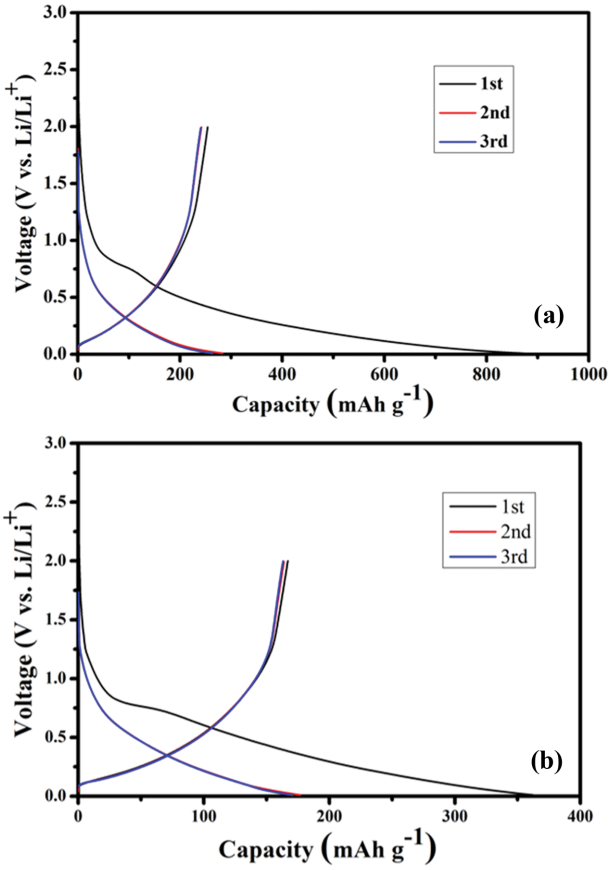

Fig. 4. Initial volgate profiles of pyrolyzed CNC at (a) 800 °C and (b) 1,600 °C composite electrodes at 100 mA g^{-1}.

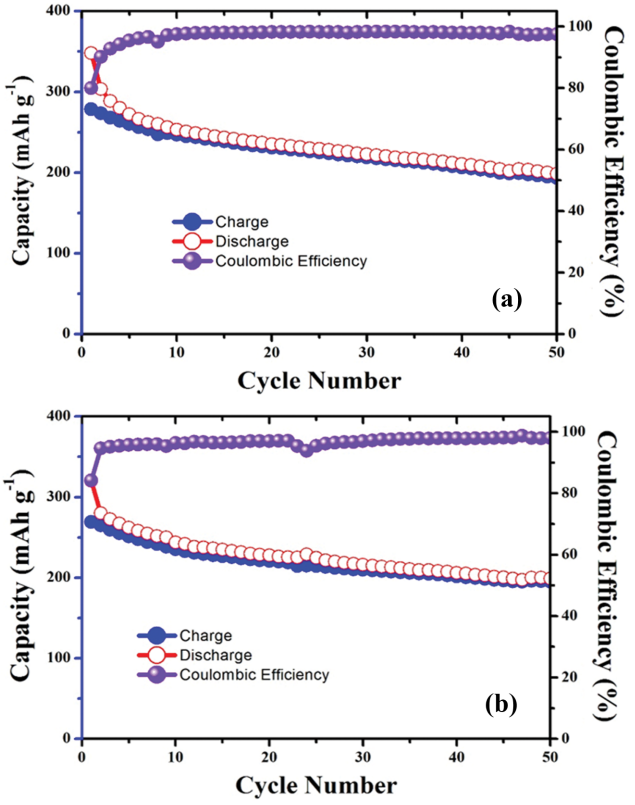

Fig. 5. Comparison of cyclic performance of pyrolyzed CNC at (a) 800 °C and (b) 1,600 °C composite electrodes at 100 mAg^{-1}.

performance of electrode. Furthermore, Fig. 2(e), (f), and (g) show the TEM images of CNC, CNC after pyrolysis at 800 °C and 1,600 °C. Indeed, the images reveal the porous surface of CNC after pyrolysis, leading to the better capacity of LIBs in comparison with bare CNC.

The Raman spectrum of CNC after pyrolysis (Fig. 3) shows peaks from 1,250 to 1,580 cm^{-1} (Raman shift) are corresponding to the D and G peak of untidiness carbon and graphitic carbon, respectively [23,24]. And the D-band and G-band are broadened and shifted for CNC-1600, and the intensity ratio of the D-band and G-band shows higher degree of graphitization in comparison with disordering of carbon, in agreement with XRD results as above.

The obtained pyrolysis CNC (CNC-800 & CNC-1600) was used as electrode in LIBs. Fig. 4 shows the initial volgate profiles at a current density of 100 mA g^{-1}. The results are 812 mAh g^{-1} for initial discharge capacity (black) and 285 mAh g^{-1} for initial charge capacity (blue), respectively in usage of CNC-800 and 365 mAh g^{-1} and 275 mAh g^{-1} are, respective, capacity for CNC-1600. Low initial Coulombic efficiency in Fig. 4 is due to the irreversible capacity loss of carbon electrode completely caused by the surface film growth due to solvent decomposition. Besides, the large irreversible capacity loss at the first cycle of the electrodes depends on electrode materials and it is a common phenomenon for LIBs.

The cycling performance and coulombic efficiency of the CNC-800 and CNC-1600 materials were also measured as shown in Fig. 5. There is a reduction in capacity from 285 mAh g^{-1} to 197 mAh g^{-1} after 50 cycles in comparison with the initial charge capacity for CNC-800 and from 275 mAh g^{-1} to 183 mAh g^{-1} after 50 cycles for CNC-1600. However, CNC electrode exhibited a stablility of capacity and the performance trend looks the same between CNC-800 and CNC-1600 electrode, and both electrodes obtained a higher capacity without pyrolysis CNC electrode. The capacity decreases slightly during the cycling and keeps the average value at 0.6% per cycle in the capacity decrease rate, which shows promising ability to get good capacity retention ratio. Polyzed CNC-800 electrode obtained better capacity than the electrode used CNC-1600, expressing 800 °C can be considered as the good temperature for CNC pyrolysis and high temperature is not nessesary for CNC pyrolysis.

Fig. 6 displays DCP curves of CNC-800 and CNC-1600 electrodes in first three cycles within 0.00 and 2.00 V potential range. The DCPs of two electrodes are comparable because of having the same component as CNC, which is also suitable for the reactions between C and Li in discharge and charge process.

The CNC-SnO_2 composite was utilized as electrode material for LIBs. Fig. 7 shows the DCPs of CNC-SnO_2 electrode for first three cycles between 0.001 and 2.00 V potential range. A difference between the first cycle and the next two cycles can be obtained from the DCPs figure. For CNC 800-SnO_2 (Fig. 7(a)), the first cycle curve shows two reduction peaks located between 0.9-1.2 and 0.5-0.7 V potential ranges. These peaks characterize the process of converting SnO_2 to Sn as to the conversion process (based on the first below shown equation) and the SEI films were formed, respec-

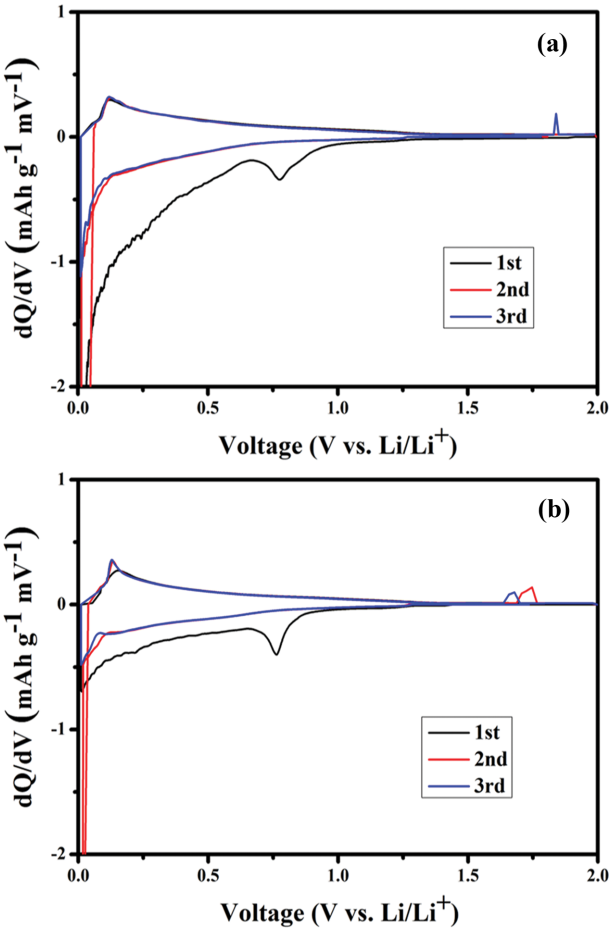

Fig. 6. DCPs of (a) 800 °C and (b) 1,600 °C pyrolyzed CNC electrodes within 0.01-2.00 V potential range.

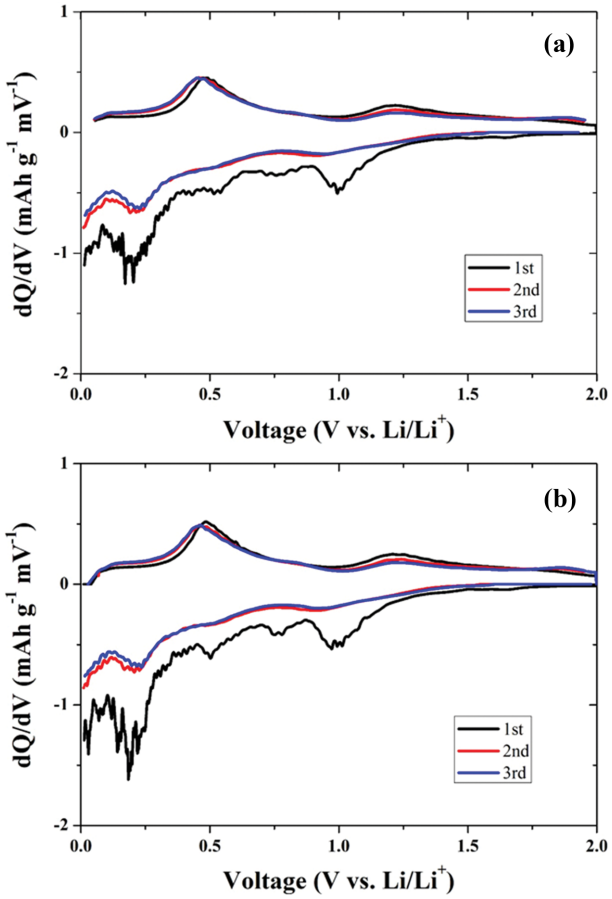

Fig. 7. DCPs of (a) CNC 800-SnO_2 and (b) CNC 1600-SnO_2 composite electrodes within 0.01-2.00 V potential range.

tively [25-28]. The lithiation (Li_xSn) of Sn (shown in Eq. (2)) can be confirmed by the peaks around 0.25 V [27]. Furthermore, with two following curves, the reduction peaks disappeared in the range of 0.5-1.5 V, which can be explained by the decomposition of electrolyte, which caused the low coulombic efficiency of first cyles (shown in the Fig. 8). The delithiation reaction of Li_xSn (shown in Eq. (3)) and the reversible changing reaction of Sn between SnO and SnO_2 (shown in Eq. (4)) can be, respectively, confirmed by two oxidation peaks at 0.6, and 1.2 V [28]. Also, the DCPs curves of CNC 1600-SnO_2 (Fig. 7(b)) between 0.001 and 2.0 V are similar to CNC 800-SNO_2. The conversion process of de/intercalating ion Li^+ can be found as follows:

$$SnO_2 + 2\,Li^+ + 2\,e^- \rightarrow Sn + Li_2O \quad (1)$$

$$Sn + x\,Li^+ + x\,e^- \rightarrow Li_xSn \quad (2)$$

$$Li_xSn \rightarrow Sn + x\,Li^+ + x\,e^- \quad (3)$$

$$Sn/SnO + Li_2O \rightarrow SnO/SnO_2 + 2\,Li^+ + 2\,e^- \quad (4)$$

The initial voltage profiles of CNC 800-SNO_2 electrode were figured out in Fig. 8(a). The capacities obtained from the first and second cycles were evaluated. The oxidation-reduction peaks of the figure show consistent results with the voltage platforms of charge-discharge. The initial discharge (black) - charge (red) capacities of CNC 800-SnO_2 are 675 and 350 mAh g^{-1}, respectively. From the observed results, it is possible that SEI film formation and the irreversible reactions of active material cause a low coulombic efficiency of 52.0% in the first cycle [29]. In comparison with the charge/discharge profiles of CNC 1600-SNO_2 shown in Fig. 8(b), the trend is the same and the initial discharge-charge capacities of CNC 1600-SnO_2 are higher at 750 and 415 mAh g^{-1}, respectively.

Fig. 9 shows the cycling performance of CNC 800-SnO_2 and CNC 1600-SNO_2. The CNC 800-SnO_2 electrode obtained a discharge capacity at 380 mAh g^{-1} after 30 cycles. On the other hand, 360 mAh g^{-1} remains to be seen at the discharge capacity of CNC 1600-SnO_2 electrode, although it have a higher initial discharge-charge capacity, which means CNC 800-SnO_2 CNC electrode exhibited a stablility of capacity.

For more information about the combination, the CNC and SnO_2 as composite materials (CNC-SnO_2) served as electrode materials in Lithium-ion batteries; the cyclic performance of pyrolyzed CNC-800, CNC-1600 (Fig. 5(a) and (b)) and CNC 800-SnO_2, CNC 1600-SnO_2 (Fig. 9(a) & (b)) were prepared. One can observe that the performance of composite materials shows greater capacity than only CNC material electrode, and the performance of CNC 800-SnO_2 shows the highest capacity. This result again confirms that 800 °C is the better temperature for CNC pyrolysis and there is no

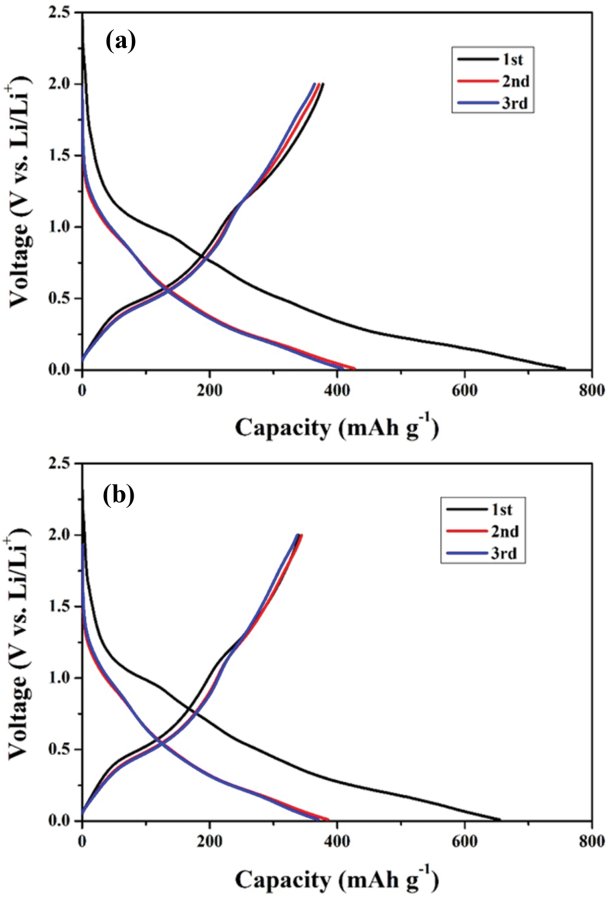

Fig. 8. Initial voltage profiles of (a) CNC 800-SnO_2 and (b) CNC 1600-SnO_2 composite electrodes at 100 mAg^{-1}.

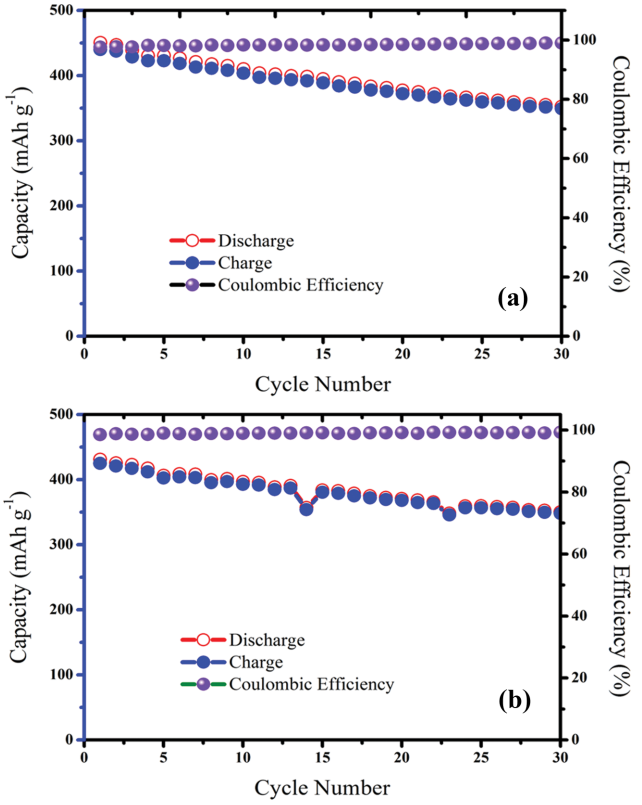

Fig. 9. Comparison of cyclic performances of (a) CNC 800-SnO_2 and (b) CNC 1600-SnO_2 composite electrodes at 100 mAg^{-1}.

need to spend more power to increase the temperature in pyrolysis process. To compare the the present work with previous reports, the electrochemical performance is summarized in Table 1. The results show that CNC-SnO_2 composite electrode provides good performance in LIBs. However, the less conductivity of CNC still affects electrode material, leading to the low capacity of LIBs.

CONCLUSION

We converted CNC into highly conductive material by pyrolysis and successfully prepared a composite CNC-SnO_2 material used as electrode materials to enhance the charge-discharge capacity and cycling performance of Li-ion battery. The discharge capacity after 30 cycles was 380 mAh g^{-1} and 220 mAh g^{-1}, respectively, for CNC 800-SnO_2 and CNC 800 electrode in Li-ion battery.

ACKNOWLEDGEMENTS

This research was financially supported by Korea Electric Power Corporation (Grant number: R18XA02) and by the Korea Institute of Energy Technology Evaluation and Planning (KETEP) and the Ministry of Trade, Industry & Energy (MOTIE) of the Republic of Korea (No. 20194030202290). We very much appreciate all measurement instruments, supported by Smart Materials Research Center for IoT in Gachon University.

REFERENCES

1. H. Zhu, W. Luo, P. N. Ciesielski, Z. Fang, J. Y. Zhu, G. Henriksson,

Table 1. Summary of C/SnO_2 composite electrochemical performance

No.	Composite	Discharge capacity	Refs.
1.	CNC-SnO_2	380 mAh g^{-1} (after 100 cycles)	Our work
2.	NC@SnO_2	750 mAh g^{-1} (after 100 cycles)	19
3.	SnO_2@ES-CCFs	506 mAh g^{-1} (after 100 cycles)	30
4.	SnO_2/C@5	656 mAh g^{-1} (after 100 cycles)	31
5.	SnO_2/C@5//NCM811	447 mAh g^{-1} (after 100 cycles)	31
6.	SnO_2-gel/cellulose	623 mAh g^{-1} (after 100 cycles)	32

M. E. Himmel and L. Hu, *Chem. Rev.*, **116**, 9305 (2016).
2. Z. Li, J. Liu, K. Jiang and T. Thundat, *Nano Energy*, **25**, 161 (2016).
3. X. Yang, K. Shi, I. Zhitomirsky and E. D. Cranston, *Adv. Mater.*, **27**, 6104 (2015).
4. L. Wang, C. Schutz, G. Salazar-Alvarez and M. M. Titirici, *RSC Adv.*, **4**, 17549 (2014).
5. X. Du, Z. Zhang, W. Liu and Y. Deng, *Nano Energy*, **35**, 299 (2017).
6. Z. Wang, R. Pan, R. Sun, K. Edstrom, M. Stromme and L. Nyholm, *ACS Appl. Energy Mater.*, **1**, 4341 (2018).
7. M. L. Foresti, A. Vazquez and B. Boury, *Carbohydr. Polym.*, **157**, 447 (2017).
8. M. C. Hsieh, C. Kim, M. Nogi and K. Suganuma, *Nanoscale*, **5**, 9289 (2013).
9. J. Lee and J. H. Moon, *Korean J. Chem Eng.*, **34**, 3195 (2017).
10. T. L. Nguyen, T. T. Salunkhe, T. N. Vo, H. W. Choi, Y. Lee, J. Choi, J. Hur and I. T. Kim, *J. Power Sources*, **414**, 470. (2019).
11. T. N. Vo, H. Kim, J. Hur, W. Choi and I. T. Kim, *J. Mater. Chem. A.*, **6**, 22645 (2018).
12. Y. Chen, J. Ma, Q. Li and T. Wang, *Nanoscale*, **5**(8), 3262 (2013).
13. S. J. R. Prabakar, Y.-H. Hwang, E.-G. Bae, S. Shim, D. Kim, M. S. Lah, K.-S. Sohn and M. Pyo, *Adv. Mater.*, **25**(24), 3307 (2013).
14. J. Deng, Y. Chen, J. Ma, E. Zhang and T. Wang, *J. Nanosci. Nanotechnol.*, **13**(6), 4297 (2013).
15. Q. Zhao, L. Ma, Q. Zhang, C. Wang and X. Xu, *J. Nanomater.*, **2015**, 6 (2015).
16. X. M. Yin, C. C. Li, M. Zhang, Q. Y. Hao, S. Liu, L. B. Chen and T. H. Wang, *J. Phys. Chem. C*, **114**(17), 8084 (2010).
17. L. B. Chen, X. M. Yin, L. Mei, C. C. Li, D. N. Lei, M. Zhang, Q. H. Li, Z. Xu, C. M. Xu and T. H. Wang, *Nanotechnol*ogy, **23**(3), 035402 (2011).
18. L. Fan, X. Li, B. Yan, J. Feng, D. Xiong, D. Li, L. Gu, Y. Wen, S. Lawes and X. Sun, *Adv. Energy Mater.*, **6**(10), 1502057 (2016).
19. J. Liang, C. Yuan, H. Li, K. Fan, Z. Wei, H. Sun and J. Ma, *Nano-Micro Lett.*, **10**, 21 (2018).
20. M. Dirican, Y. Lu, Y. Ge, O. Yildiz and X. Zhang, *ACS Appl. Mater. Interfaces*, **7**(33), 18387 (2015).
21. B. Huang, X. Li, Y. Pei, S. Li, X. Cao, R. C. Massé and G. Cao, *Small*, **12**(14), 1945 (2016).
22. S. Kuga, D. Y. Kim, Y. Nishiyama and R. M. Brown, *Mol. Cryst. Lip. Cryst.*, **387**, 13 (2002).
23. Z. Lin, X. Xiong, J. Zheng, G. Wang and C. Yang, *Mater. Lett.*, **202**, 123 (2017).
24. Y. Luo, X. Zhou, Y. Zhong, M. Yang, J. Wei and Z. Zhou, *Electrochim. Acta*, **154**, 136 (2015).
25. C. Zhu, X. Xia, J. Liu, Z. Fan, D. Chao, H. Zhang and H. J. Fan, *Nano Energy*, **4**, 105 (2014).
26. B. Jiang, Y. He, B. Li, S. Zhao, S. Wang, Y. B. He and Z. Lin, *Angew. Chem. Int. Ed.*, **56**(7), 1869 (2017).
27. M. Zhang, Z. Sun, T. Zhang, D. Sui, Y. Ma and Y. Chen, *Carbon*, **102**, 32 (2016).
28. R. Li, B. Wang, S. Ji and P. Jin, *RSC Adv.*, **6**(59), 54179 (2016).
29. R. Hu, Y. Ouyang, T. Liang, H. Wang, J. Liu, J. Chen, C. Yang, L. Yang and M. Zhu, *Adv. Mater.*, **29**(13), 1605006 (2017).
30. S. I. Oh, J. C. Kim and D. W. Kim, *Cellulose*, **26**, 2557 (2019).
31. Z. Chen, Z. Xu, W. Li, C. Chen, J. Yang, J. Liu, F. Gong, J. Liao and M. Wu, *ACS Appl. Energy Mater.*, **2**, 5171 (2019).
32. M. Wang. S. Li, Y. Zhang and J. Huang, *Chem. Eur. J.*, **21**, 16195 (2015).